Ultrafast heat-assisted magnetization dynamics in a ferrimagnetic insulator

A. Dolgikh,[1] D. Afanasiev,[1] V. V. Yurlov,[2,3] M. V. Logunov,[4] A. K. Zvezdin,[3,5,6] and A. V. Kimel[1]

[1]*Radboud University, Institute for Molecules and Materials, Nijmegen 6525AJ, Netherlands*
[2]*Moscow Institute of Physics and Technology, 141700 Dolgoprudny, Russia*
[3]*New Spintronic Technologies, 121205 Moscow, Russia*
[4]*Kotel'nikov Institute of Radio Engineering and Electronics, Russian Academy of Science, 119991 Moscow, Russia*
[5]*Prohorov General Physics Institute, Russian Academy of Sciences, 125009 Moscow, Russia*
[6]*Lebedev Physical Institute of the Russian Academy of Science, 119991 Moscow, Russia*

(Received 9 November 2022; revised 16 February 2023; accepted 3 March 2023; published 21 March 2023)

Ultrafast laser-induced heating of ferrimagnetic iron garnet in an external magnetic field triggers magnetization precessional dynamics with a large amplitude. The dynamics is studied as a function of magnetic field, laser fluence, and sample temperature. Exploring the three-dimensional space of these parameters experimentally and computationally, we identify the conditions for which the amplitude of the precession is the largest and even achieves values sufficient for magnetic recording. We found that the range of external magnetic fields and temperatures, which corresponds to the magnetic recording, is rather narrow. Modeling the dynamics, using magnetization as a macroscopic parameter, reveals that this range of parameters is defined by the optimal height of the potential barrier separating two stable states. The barrier needs to be low enough to allow the switching but not so low that the stability of the states is lost.

DOI: 10.1103/PhysRevB.107.094424

I. INTRODUCTION

Ultrafast magnetism is a rapidly developing research field that explores spin dynamics in ferromagnetic, ferrimagnetic, and antiferromagnetic media excited by sub-100 ps stimuli [1–6]. If such stimuli excite magnets on a time scale faster than the characteristic times of elementary spin-lattice or electron-lattice interactions, they bring the media into a strongly nonequilibrium state, where the conventional description of magnetic phenomena in terms of equilibrium thermodynamics is no longer valid, conventional approximations fail, and the triggered magnetization dynamics can become counterintuitive [4]. Apart from purely fundamental interest, ultrafast magnetism challenges the fundamental and practical limits on the speed and energy dissipations of writing of a single magnetic bit [7–10]. Hence, the field has the potential to impact future data storage technologies.

Among all magnetic materials studied in ultrafast magnetism, ferrimagnets represent a rich and probably the most appealing playground to explore large amplitude magnetization dynamics and magnetic writing induced by ultrashort stimuli. For instance, in contradiction with Curie's symmetry principle, it was discovered that solely ultrafast heating, either with the help of femtosecond and picosecond laser pulses [11–15] or picosecond electrical pulses [16], can reverse the magnetization of ferrimagnetic metals. Although it has been believed that heat-assisted magnetization dynamics and recording in insulators are slow [3], ferrimagnetic iron garnets facilitate an unconventional, precessional route of heat-assisted magnetic recording [17]. In this mechanism, laser-induced heating destroys magnetic anisotropy, launches anomalously damped magnetization precession in an external magnetic field, and eventually results in capturing of the magnetization by another stable bit state [17]. In ferrimagnets, where both the net magnetization and magnetic anisotropy are strongly temperature dependent, the efficiency of the heat-assisted precessional magnetic recording must be a function not only of magnetic field but also of temperature. The goal of this paper is to reveal the mutual interplay of temperature and magnetic field which eventually leads to laser-induced switching.

In this paper, we study large-amplitude heat-assisted magnetization dynamics in ferrimagnetic iron garnet by performing time-resolved single-shot imaging of magnetization dynamics as a function of external magnetic field, laser fluence, and sample temperature. Exploring the three-dimensional space of these parameters experimentally and computationally, we identify and explain the conditions for which the amplitude of the precession is the largest and even achieves values sufficient for magnetic recording.

This paper is organized as follows. Section II describes the properties of the material investigated, together with the employed experimental techniques. Section III summarizes experimental results. Section IV describes the employed theoretical model and the results of the simulations, compares them with the experimental results, and eventually interprets the latter. The paper is concluded by Sec. V.

II. SAMPLE AND EXPERIMENTAL SETUP

Here, we studied heat-assisted magnetization dynamics in ferrimagnetic lutetium iron garnet $(Bi_{0.8}, Lu_{2.8})_3(Fe_{3.2}, Ga_1, Al_{0.8})_5O_{12}$. In this compound, the spins of Fe^{3+} ions in the octahedral and tetrahedral sites form two nonequivalent magnetic sublattices with oppositely oriented magnetizations $\mathbf{M}_1$ and $\mathbf{M}_2$, respectively.

The difference in the volume fraction of the octahedral and tetrahedral sites leads to a nonzero net magnetization $\mathbf{M} = \mathbf{M}_1 + \mathbf{M}_2$ below the Curie temperature $T_C \approx 600\,\mathrm{K}$ [18]. In the parent compound $Lu_3Fe_5O_{12}$, the net magnetization is dominated by the tetrahedral sublattice. Substituting Fe^{3+} ions in the tetrahedral positions with Ga^{3+} and Al^{3+} levels off the magnetizations of the sublattices such that, at the magnetization compensation point $T_M = 50\,\mathrm{K}$, the magnetizations of the sublattices cancel each other such that $\mathbf{M}_1(T_M) = -\mathbf{M}_2(T_M)$ and the net magnetization vanishes $\mathbf{M} = 0$. We note that neither Lu^{3+} nor Bi^{3+} has a magnetic moment, and thus, they have no impact on the net magnetization $\mathbf{M}$. However, the magneto-optical Faraday effect depends not only on the magnetization but also on the Verdet constant. Adding Bi^{3+} ions increases the Verdet constant [19–22] but is known to change T_C as a side effect [23].

The epitaxial film of iron garnet with a thickness of $8\,\mu\mathrm{m}$ was grown on a (111) $Gd_3Ga_5O_{12}$ substrate using liquid-phase epitaxy. Although crystals of iron garnet have a cubic magnetic anisotropy, thin films normally acquire a uniaxial anisotropy during growth, with the easy axis along the sample normal. At room temperature, the magnetization can be saturated by applying a magnetic field of about $H_s = 50\,\mathrm{Oe}$ along the easy axis [24]. The film of iron garnet is characterized by a strong magneto-optical Faraday effect reaching 6° for light at the wavelength of $800\,\mathrm{nm}$ ($h\nu = 1.55\,\mathrm{eV}$). The magneto-optical effect at this wavelength is dominated by the magnetization of the Fe^{3+} ions of the octahedral sublattice [22].

To study laser-induced magnetization dynamics in the iron garnet, we employed time-resolved single-shot magneto-optical imaging. To trigger magnetization dynamics, we employed a femtosecond laser pulse having a 100-fs duration at the central wavelength of 625 nm ($h\nu = 1.98\,\mathrm{eV}$). We experimentally estimated the absorption coefficient at this wavelength to be $\sim 300\,\mathrm{cm}^{-1}$. Hence, the light penetration depth ($40\ \mu\mathrm{m}$) is still substantially larger than the sample thickness. This condition ensures a nearly homogeneous pump-induced heating across the whole sample thickness.

The linearly polarized pump beam was at the angle of incidence of 20° and was focused into a spot with the width at half maximum equal to $100\ \mu\mathrm{m}$. A magneto-optical image of the sample was obtained using linearly polarized probe pulses with a duration of ~ 100 fs at the central wavelength of 800 nm. The unfocused probe beam at normal incidence was used to visualize spatial dynamics induced by the pump pulse. Due to the magneto-optical Faraday effect, the component of the magnetization normal to the sample plane M_z results in a polarization rotation of the probe pulses $\alpha_F \sim M_z$. Using an optical analyzer, we transform the polarization rotation into intensity changes, which are subsequently detected by a charge-coupled device (CCD) camera [Fig. 1(a)]. This experimental scheme enables visualization of spatial distribution of the sample magnetization and is characterized by a particular sensitivity to the out-of-plane magnetization component. With varying time delay between the pump and probe pulses, one can obtain time-resolved magneto-optical snapshots of the pump-induced magnetization dynamics with a temporal resolution down to 100 fs.

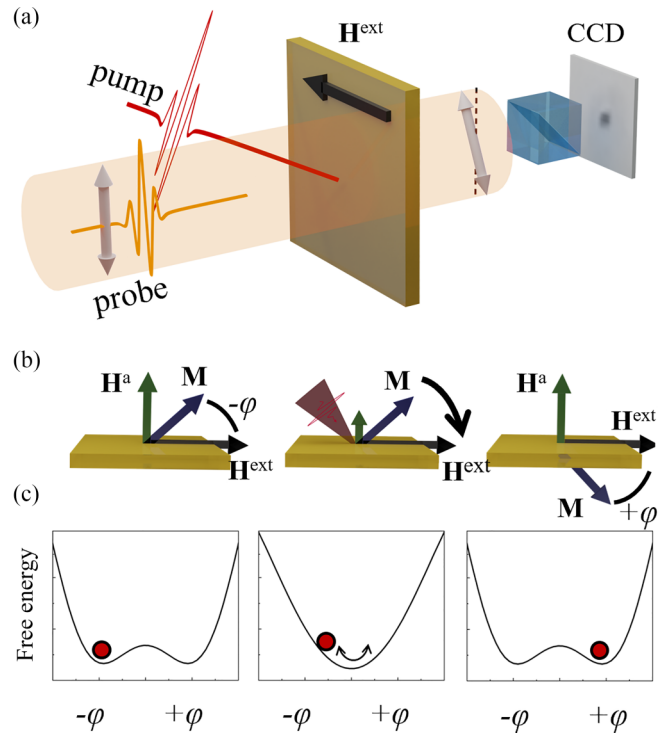

FIG. 1. (a) A schematics of the experiment: unfocused probe illuminates the sample; rotation of the probe polarization plane α_F is detected by the charge-coupled device (CCD) camera. (b) Evolution of the sample magnetic state. From left to right: unperturbed state; pump pulse heats the sample, reduces the field of magnetic anisotropy H^a and thus launches magnetization precession; after relaxation, H^a is restored, and the magnetization $\mathbf{M}$ is fixed in the switched direction. (c) The free energy profile corresponds to the cartoons in (b).

The measurements were performed for a wide range of magnetic fields H^{ext} such that $0 < H^{ext} < 3.5\,\mathrm{kOe}$. The field was applied in the sample plane, leading to a tilt of the magnetization from the sample normal. For the field applied exactly in the sample plane, the magnetization has two equivalent energy minima of thermodynamic potential corresponding to magnetizations oriented at angles $+\varphi$ and $-\varphi$ with respect to the sample plane, see Fig. 1(b). Here, $\varphi = 0$ corresponds to the peak of the potential barrier separating the minima. It means that, if the magnetization has deviated from one minimum over an angle larger than φ, there is a chance that, upon relaxation, the magnetization will relax to another minimum. In this case, the whole procedure will resemble the recording of a single magnetic bit, as explained in Ref. [17]. A slight tilt of the magnetic field out of the sample plane breaks the equivalence between the potential minima such that, at $H_z^{ext} > H_s$, one of the minima eventually disappears, and the magnetization saturates. In this paper, we intentionally tilted the external magnetic field over an angle of $\sim 0.5^\circ$ from the sample plane. The tilted field did not destroy the second minimum but ensured that, if the magnetization is switched under an action of a single pump pulse, it relaxes back to the initial state before the next pump pulse arrives.

Figure 2 shows the magneto-optic Faraday effect α_F as a function of the applied magnetic field in the geometry of the

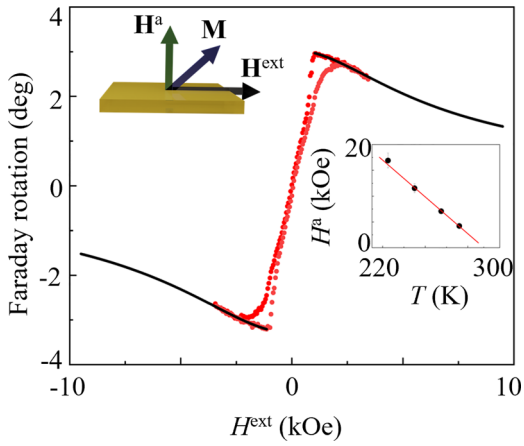

FIG. 2. The probe polarization rotation vs the external magnetic field at $T = 275$ K. Experimental data are represented by red circles, black lines extrapolate the dependence to high magnetic fields. For the extrapolation, we fit the experimented data points for $H^{\text{ext}} > H_s$ with function $\alpha_{\text{F}} = A\cos\varphi$, where A is a fit parameter and $\varphi = \arctan\frac{H^a}{H^{\text{ext}}}$ is obtained as explained in the text. The inset shows the estimated H^a as a function of temperature as explained in the text.

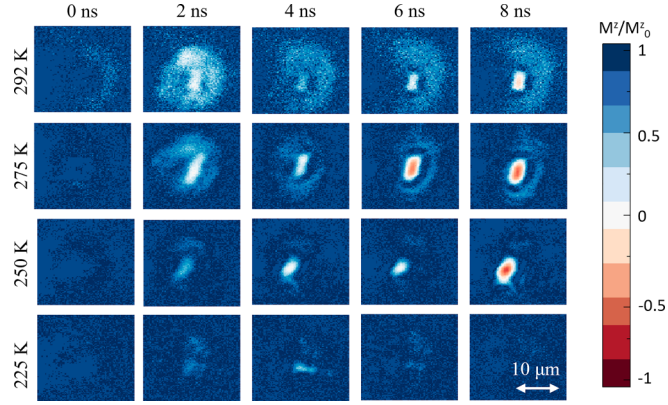

FIG. 3. Temporally and spatially resolved laser-induced magnetization dynamics.

experiment. Due to the small out-of-plane z component of the magnetic field, the magnetization is saturated along the easy axis. Hence, the maximum value of the Faraday effect $\alpha_{\text{F}}^{\max}$ (Fig. 2) corresponds to the case when the magnetization is aligned along the normal to the sample. A stronger external field pulls the magnetization toward the sample plane, which is seen as a negative slope for the fields $H^{\text{ext}} > 1$ kOe when $H_z^{\text{ext}} > H_s$. Using the slope, we estimated the effective field of magnetic anisotropy H^a. Assuming that the equilibrium orientation of the magnetization is defined by an interplay between the mutually perpendicular external magnetic field and the effective field of magnetic anisotropy, the slope from Fig. 2 was fitted using

$$\alpha_{\text{F}} = \alpha_{\text{F}}^0 \cos\left[\arctan\left(\frac{H^{\text{ext}}}{H^a}\right)\right], \tag{1}$$

where α_{F}^0 is the Faraday rotation of the saturated sample, i.e., the maximum rotation. The anisotropy fields H^a were estimated from the measured hysteresis loops as a function of temperature, and the results are summarized in the inset of Fig. 2. Applying linear fit to the data and extrapolating the fitted function to higher temperatures suggests that the anisotropy field can even reach zero far below T_{C}. Such behavior appears to be typical for this type of ferrimagnetic iron garnet [23].

III. EXPERIMENTAL RESULTS

Figure 3 shows time-resolved magneto-optical images of the magnetization dynamics excited by an intense femtosecond pump with the fluence of 80 mJ/cm^2. The measurements were performed in a magnetic field $H^{\text{ext}} = 3$ kOe at several temperatures above T_{M}. It is seen that, during the first few nanoseconds, the laser-induced dynamics evolves in a large area. Starting from 4 ns, one observes an onset of an intense signal in an area ~ 7 μm in diameter just in the center of the spot. This area is surrounded by a ring with a weaker signal resembling a bull's eye pattern much like those reported in Refs. [7,17,25]. To process the magneto-optical data, we calculated the z component of the magnetization after the pump excitation M^z normalized on M_0^z. The changes of M^z/M_0^z by $>100\%$ imply that the amplitude of the magnetization dynamics is sufficiently large to overcome the potential barrier separating two energy minima, see Fig. 1(c). Digitizing the images, we obtain quantitative data on the magnetization dynamics. We chose an area inside the spot with the largest and seemingly homogeneous magneto-optical signal for the delay of $\sim$8 ns. Integrating the signal in this area, we obtain a measure of the net magnetization, which we plot as a function of time for various temperatures (see Fig. 4). To account for the nonlinear character of the dependence between the inten-

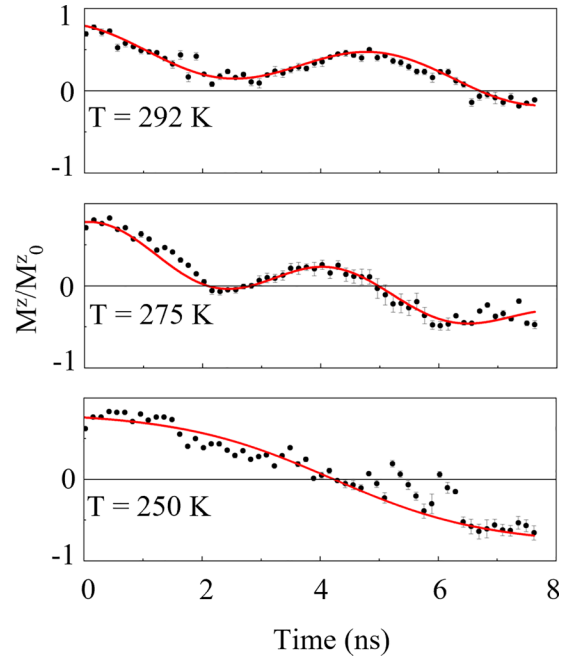

FIG. 4. Pump-induced traces of magnetization dynamics obtained by spatial integration of the images shown in Fig. 3 as explained in the text. The red lines are guides to the eye shown to emphasize the fact of the oscillations.

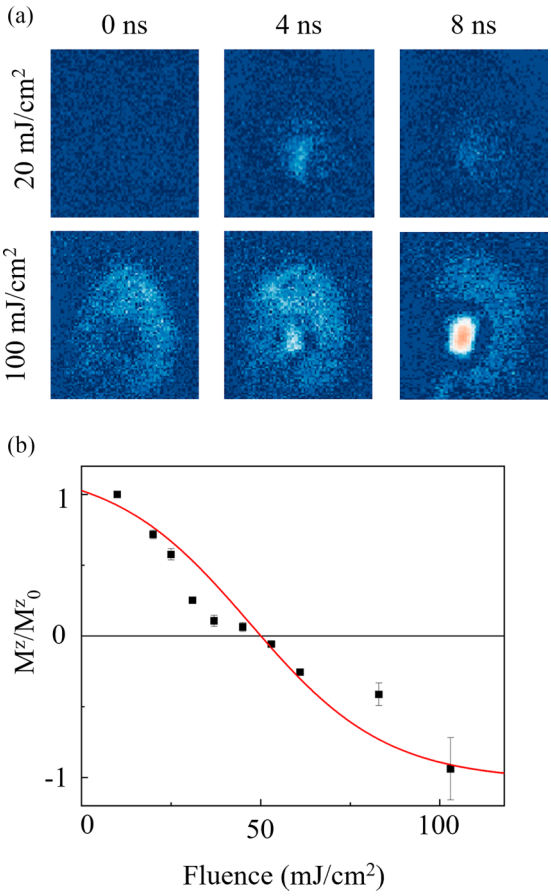

FIG. 5. (a) Temporarily and spatially resolved magnetization dynamics for low $F = 20$ mJ/cm^2 (upper panel) and high $F = 100$ mJ/cm^2 pump fluence (lower panel), respectively. (b) Out-of-plane component of the magnetization at 8 ns after pump pulse. $M^z/M_0^z = 1$ corresponds to the magnetization in the initial state (up). $M^z/M_0^z = -1$ corresponds to the reversed state (down). The red line is a guide to the eye shown to highlight the nonlinear character of the dependence.

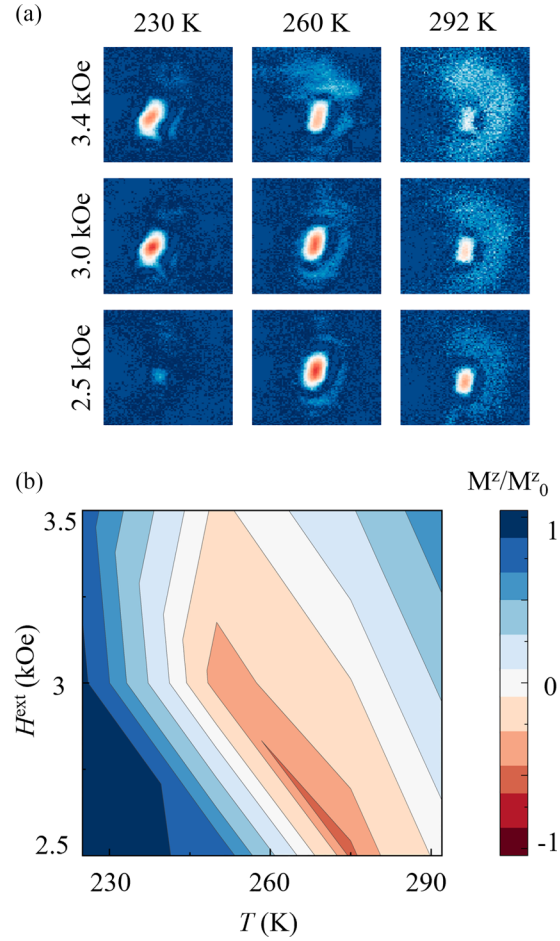

FIG. 6. (a) The magneto-optical images obtained 8 ns after the pump for various temperatures (horizontal) and magnetic fields (vertical). The pump fluence is 80 mJ/cm^2. (b) Phase diagram of the pump-induced magnetization state as obtained after digitizing the images shown in (a).

sity detected by the camera and the Faraday rotation proving information about M^z, we followed the routine described in Ref. [26]. The dynamics reveals such a fingerprint of precessional magnetic switching as oscillations of the magnetization with a large amplitude. The signal in the center of the images corresponds to the rotation of the magnetization over a large angle, which can even exceed φ [see Fig. 1(b)]. According to Ref. [17], such a large amplitude of the magnetization precession can be sufficient for switching. The switching amplitudes are observed only in a narrow temperature range between 250 and 292 K, pointing to the heat-assisted nature of the pump-induced changes.

The pump fluence is 80 mJ/cm^2. Magnetic field $H^{\text{ext}} = 3$ kOe is applied in the sample plane. The color code represents the orientation of the magnetization such that magnetization pointing up corresponds to blue (1), while magnetization pointing down corresponds to red (-1).

The upper and lower panels of Fig. 5(a) show magnetization dynamics for low and high pump fluences, respectively. Even measuring the magnetization dynamics up to 8 ns for a low pump fluence, switching is revealed only after strong pump excitation. Figure 5(b) summarizes amplitudes of the precessional dynamics as a function of fluence and highlights its nonlinear character.

Finally, to summarize the conditions necessary for the switching, we built up a phase diagram showing snapshots of the photo-induced magnetic changes at long time delays after the pumping. Figure 6(b) summarizes the snapshots obtained at the pump-probe delay $\Delta t = 8$ ns for various temperatures and external magnetic fields. Note that, while for some combinations of H^{ext} and T the changes of M^z/M_0^z exceed 100% ($M^z/M_0^z \leqslant 0$), there are also regions where the magnetization was impacted only slightly. Moreover, the largest changes in the magnetization are achieved along one diagonal of the square formed by the horizontal (T) and the vertical (H^{ext}) axes.

IV. DISCUSSION

Our results show that large amplitude magnetization dynamics and switching in the studied iron garnet are strongly dependent on temperature and magnetic field. Although the

geometry of the experiment and the mechanism of the switching are like those described in Ref. [17], in this paper, we reveal that the magnetization dynamics depends not only on the external magnetic field and laser fluence but also on temperature. To understand the origin of this dependence, we carried out a set of numerical simulations.

In the mechanism described in Ref [17], ultrafast laser-induced heating destroys the magnetic anisotropy, thus changing the equilibrium orientation of the magnetization. To reach the new equilibrium, the magnetization starts a large-amplitude precession around the external magnetic field. Due to damping, the magnetization can be caught by the second stable state. We estimated the temperature increase produced by the laser pulse using the heat balance equation:

$$\Delta T = \frac{\alpha F S}{cm}, \tag{2}$$

where S and m are the surface area and the mass of the irradiated sample, c is the specific heat, and α is the absorption coefficient. The specific heat c and the mass density of the garnet were taken from Refs. [27–31], and α was estimated experimentally with the help of the Beer-Lambert law. Considering a Gaussian profile of the pump intensity, the pump fluence of 80 mJ/cm^2 must be enough to increase the sample temperature for ∼20 K. According to the data shown in the inset of Fig. 2, such heating is indeed large enough to weaken and nearly destroy the magnetic anisotropy in the sample.

We assume that the dynamics could be described using magnetization as the only macroscopic order parameter. While such an approximation overlooks the multisublattice nature of the iron garnet, it can be used far from the compensation temperature T_M [32]. The dynamics is further described using the Lagrange formalism and the Rayleigh dissipation function [33–35]:

$$\begin{aligned}\mathcal{L} &= M(1-\cos\theta)\frac{\dot{\varphi}}{\gamma} - \mathcal{U}(\theta,\varphi), \mathcal{U}(\theta,\varphi)\\ &= -\frac{1}{2}MH^{\mathrm{A}}(T)\sin^2\theta\sin^2\varphi - MH_{\parallel}^{\mathrm{ext}}\cos\theta\\ &\quad - MH_{\perp}^{\mathrm{ext}}\sin\theta\sin\varphi, \mathcal{R}\\ &= \frac{\alpha_{\mathrm{d}}(\dot{\theta}+\sin^2\theta\varphi^2)}{\gamma},\end{aligned} \tag{3}$$

where $\mathcal{U}(\theta,\varphi)$ is potential energy, M is the total magnetization of the magnetic film, γ is the gyromagnetic ratio, φ and θ are azimuthal and polar angles of the magnetization vector, respectively, α_d is the Gilbert damping parameter, and $H_{\parallel}^{\mathrm{ext}}$ and $H_{\perp}^{\mathrm{ext}}$ are in-plane and out-of-plane components of the applied magnetic field, respectively. The first term in the potential energy represents the anisotropy energy, the second and the third the Zeeman energy. From the potential energy, one finds two ground states of the system corresponding to the angles: $\varphi^{(1)} = \frac{\pi}{2}, \theta^{(1)} \approx \arccos[\frac{H^{\mathrm{ext}}}{H^a(T)}]$ and $\varphi^{(2)} = \frac{3\pi}{2}, \quad \theta^{(2)} \approx \arccos[\frac{H^{\mathrm{ext}}}{H^a(T)}]$, respectively. Using Eq. (1), the Euler-Lagrange equations can be written as follows:

$$\begin{aligned}\dot{\theta} + \alpha\sin\theta\dot{\varphi} &= \frac{\omega_a(T)\sin\theta\sin 2\varphi}{2} + \omega_{\mathrm{H}}^{\perp}\cos\varphi\\ \sin\theta\dot{\varphi} - \alpha\dot{\theta} &= -\frac{\omega_a(T)\sin^2\varphi\sin 2\theta}{2}\\ &\quad + \omega_{\mathrm{H}}^{\parallel}\sin\theta - \omega_{\mathrm{H}}^{\perp}\cos\theta\sin\varphi,\end{aligned} \tag{4}$$

where $\omega_a(T) = \gamma H^a(T)$, $\omega_{\mathrm{H}}^{\parallel} = \gamma H_{\parallel}^{\mathrm{ext}}$, $\omega_{\mathrm{H}}^{\perp} = \gamma H_{\perp}^{\mathrm{ext}}$. The temperature of the magnetic film changes in time $T = T(t)$ due to laser pulse heating. To model the time dependence, we solve the power balance equation:

$$\chi F = C_{\mathrm{V}} V\frac{dT}{dt} + c(T - T_0), \tag{5}$$

where F is the laser fluence, C_{V} is the isochoric specific heat, V is the volume of the heated area, T_0 is the bias temperature of the substrate, χ and c are material parameters whose ratio can be defined by fitting experimental data assuming that $\Delta T \approx \lambda F$, where $\lambda = 0.25\,\mathrm{K}\cdot\mathrm{cm}^2/\mathrm{mJ}$ was calculated from Eq. (2), $\Delta T = T(\tau) - T_0$, and τ is the pulse duration. This model implicitly assumes instantaneous heat transfer from light to the lattice. Indeed, it is known in optically excited magnetic dielectrics, such as iron garnets [3,36,37], that the energy from optically excited electrons to the lattice is transferred at the subpicosecond timescale. Afterwards, the equilibrium lattice temperature is established at the time scale of thermalization of phonons, which is given by the characteristic time of phonon-phonon interaction (∼100 ps). As this time scale is much shorter than the characteristic time scales of the spin precession presented in this paper, the assumption of instantaneous heating holds true for the modeling of magnetization dynamics.

We performed the modeling by taking the states with $\varphi = \varphi^{(1)} = \frac{\pi}{2}, \quad \theta = \theta^{(1)}$ as the initial state. The second metastable state is thus $\varphi = \varphi^{(2)} = \frac{3\pi}{2}, \ \theta = \theta^{(2)}$. In the modeling, we also set that $\alpha_d = 0.05$, $\frac{H_{\perp}}{H_{\parallel}} = 0.01$, $V = 6.3\times 10^4\,\mu\mathrm{m}^3$, $C_{\mathrm{V}} = 4.1\,\mathrm{J/K\,cm}^3$, and $F = 80\,\mathrm{mJ/cm}^2$. The temperature dependence of the anisotropy field $H^a(T)$ is taken from the experiment (see Fig. 2).

Figure 7(a) summarizes combinations of the applied magnetic fields and the bias temperatures for which the laser-induced magnetization dynamics eventually results in the switching of the magnetization between two stable states. At a fixed magnetic field, the switching is possible only in a relatively narrow range of temperatures. This range shifts to lower temperatures upon an increase in the strength of the applied magnetic field. Indeed, a temperature increase results in a decrease in the anisotropy field H^a. To preserve the conditions leading to the switching, upon an increase of the bias temperature, the applied magnetic field must be decreased. Upon even further increase of the bias temperature, the magnetic anisotropy does not result in a potential barrier between the initial and the final states any longer and the concept of switching loses its sense. Figure 7(b) shows the route of the precessional dynamics on the unit sphere for three different areas of the diagram from Fig. 7(a). The corresponding profiles of the free energy and the trajectories of the magnetization are presented in Fig. 7(c), respectively. The results of the model-

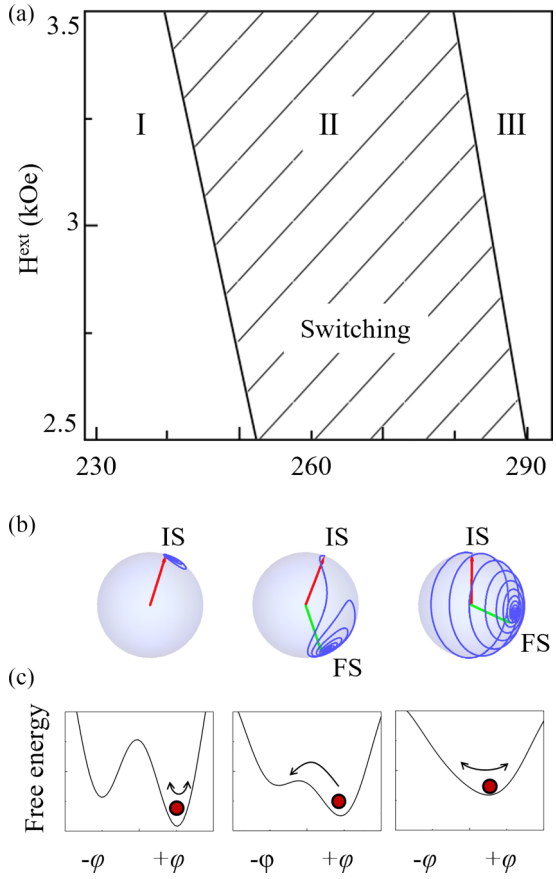

FIG. 7. (a) Calculated *H-T* diagram of the final magnetization state. Hatched area corresponds to the reversed magnetization. Three types of dynamics (I–III) are described using (b) three-dimensional (3D) trajectories and (c) free energy profiles. The symbols IS and FS on the trajectories stand for the initial and final states, respectively.

ing are in good qualitative agreement with the experimental data shown in Fig. 6. However, the experimentally observed range of temperatures at which the switching is possible is much narrower than the one in theory. This discrepancy can be explained by the fact that our simple model does not account for stochastic magnetic fields randomly affecting spins in a magnet at nonzero temperatures. Inhomogeneous heating across the sample thickness also can be a reason for the observed differences between the experiment and modeling.

V. CONCLUSIONS

Using femtosecond laser pulses and laser-induced heating, we have experimentally explored heat-assisted magnetization dynamics in external magnetic fields and variable temperatures. More particularly, we reveal how the magnetization dynamics depends on magnetic field, laser fluence, and sample temperature. We demonstrate that heat-assisted magnetic recording can, in principle, be realized only in a relatively narrow range of the parameters. Modeling the dynamics using magnetization as a macroscopic order parameter, we show that this range of the parameters is defined by the optimal height of the potential barrier separating two bit states. We show that, to achieve deterministic switching, the optimal height of the barrier is required. It should be low enough to allow the switching. At the same time, if the barrier height is reduced further, the stability of the bit states is lost, and two minima cannot be distinguished any longer.

ACKNOWLEDGMENTS

The authors thank C. Berkhout and S. Semin for technical support. This paper has received funding from de Nederlandse Organisatie voor Wetenschappelijk Onderzoek (NWO) and innovation program under the European Union's Horizon 2020 research and innovation program under the Marie Skłodowska-Curie Grant Agreement No. 861300 (COMRAD), from the COST Action CA17123 "Ultrafast opto-magneto-electronics for non-dissipative information technology" (MAGNETOFON). M.V.L. is supported by the Government of the Russian Federation for state support of scientific research conducted under guidance of leading scientists (Project No. 075-15-2022-1098). V.V.Y. and A.K.Z. are supported by Russian Science Foundation Grant No. 22-12-00367.

[1] E. Beaurepaire, J. C. Merle, A. Daunois, and J. Y. Bigot, Phys. Rev. Lett. **76**, 4250 (1996).
[2] C. D. Stanciu, F. Hansteen, A. V. Kimel, A. Kirilyuk, A. Tsukamoto, A. Itoh, and T. Rasing, Phys. Rev. Lett. **99**, 047601 (2007).
[3] A. V. Kimel, R. V. Pisarev, J. Hohlfeld, and T. Rasing, Phys. Rev. Lett. **89**, 287401 (2002).
[4] A. Kirilyuk, A. V. Kimel, and T. Rasing, Rev. Mod. Phys. **82**, 2731 (2010).
[5] J. Stöhr and H. C. Siegmann, *Solid-State Sciences* (Springer, Berlin, 2006), Vol. 5, p. 236.
[6] A. V. Kimel, A. M. Kalashnikova, A. Pogrebna, and A. K. Zvezdin, Phys. Rep. **852**, 1 (2020).
[7] I. Tudosa, C. Stamm, A. B. Kashuba, F. King, H. C. Siegmann, J. Stöhr, G. Ju, B. Lu, and D. Weller, Nature (London) **428**, 831 (2004).
[8] K. Hono, Y. K. Takahashi, G. Ju, J.-U. Thiele, A. Ajan, X. Yang, R. Ruiz, and L. Wan, MRS Bull. **43**, 93 (2018).
[9] M. Kief and R. Victora, MRS Bull. **43**, 87 (2018).
[10] M. H. Kryder, E. C. Gage, T. W. McDaniel, W. A. Challener, R. E. Rottmayer, G. Ju, Y.-T. Hsia, and M. F. Erden, Proc. IEEE **96**, 1810 (2008).
[11] A. V. Kimel and M. Li, Nat. Rev. Mater. **4**, 189 (2019).
[12] C. S. Davies, T. Janssen, J. H. Mentink, A. Tsukamoto, A. V. Kimel, A. F. G. van der Meer, A. Stupakiewicz, and A. Kirilyuk, Phys. Rev. Appl. **13**, 024064 (2020).
[13] C. Banerjee, N. Teichert, K. E. Siewierska, Z. Gercsi, G. Y. P. Atcheson, P. Stamenov, K. Rode, J. M. D. Coey, and J. Besbas, Nat. Commun. **11**, 4444 (2020).
[14] T. A. Ostler, J. Barker, R. F. L. Evans, R. W. Chantrell, U. Atxitia, O. Chubykalo-Fesenko, S. El Moussaoui, L. Le

Guyader, E. Mengotti, L. J. Heyderman *et al.*, Nat. Commun. **3**, 666 (2012).
[15] J. H. Mentink, J. Hellsvik, D. V. Afanasiev, B. A. Ivanov, A. Kirilyuk, A. V. Kimel, O. Eriksson, M. I. Katsnelson, and Th. Rasing, Phys. Rev. Lett. **108**, 057202 (2012).
[16] Y. Yang, R. B. Wilson, J. Gorchon, C. H. Lambert, S. Salahuddin, and J. Bokor, Sci. Adv. **3**, 1603117 (2017).
[17] C. S. Davies, K. H. Prabhakara, M. D. Davydova, K. A. Zvezdin, T. B. Shapaeva, S. Wang, A. K. Zvezdin, A. Kirilyuk, Th. Rasing, and A. V. Kimel, Phys. Rev. Lett. **122**, 027202 (2019).
[18] V. J. Fratello, S. E. G. Slusky, C. D. Brandle, and M. P. Norelli, J. Appl. Phys. **60**, 2488 (1986).
[19] G. Scott and D. Lacklison, IEEE Trans. Magn. **12**, 292 (1976).
[20] V. Doormann, J. P. Krumme, and H. Lenz, J. Appl. Phys. **68**, 3544 (1990).
[21] I. A. Dolgikh, F. Formisano, K. H. Prabhakara, M. V. Logunov, A. K. Zvezdin, P. C. M. Christianen, and A. V. Kimel, Appl. Phys. Lett. **120**, 012401 (2022).
[22] W. A. Crossley, R. W. Cooper, J. L. Page, and R. P. van Stapele, Phys. Rev. **181**, 896 (1969).
[23] P. Hansen, C.-P. Klages, J. Schuldt, and K. Witter, Phys. Rev. B **31**, 5858 (1985).
[24] M. V. Gerasimov, M. V. Logunov, A. V. Spirin, Y. N. Nozdrin, and I. D. Tokman, Phys. Rev. B **94**, 014434 (2016).
[25] C. H. Back, D. Weller, J. Heidmann, D. Mauri, D. Guarisco, E. L. Garwin, and H. C. Siegmann, Phys. Rev. Lett. **81**, 3251 (1998).
[26] Y. Hashimoto, A. R. Khorsand, M. Savoini, B. Koene, D. Bossini, A. Tsukamoto, A. Itoh, Y. Ohtsuka, K. Aoshima, A. V. Kimel *et al.*, Rev. Sci. Instrum. **85**, 063702 (2014).
[27] A. B. Harris and H. Meyer, Phys. Rev. **127**, 101 (1962).
[28] M. Khoshakhlagh, J. Islamian, S. Abedi, and B. Mahmoudian, World J. Nucl. Med. **14**, 156 (2015).
[29] M. Guillot, F. Tchéou, A. Marchand, P. Feldmann, and R. Lagnier, Z. Phys. B: Condens. Matter **44**, 53 (1981).
[30] T. B. Mirianashvili, V. S. Varazashvili, M. S. Tsarakhov, and T. A. Pavlenishvili, Zh. Neorg. Khim. **42**, 1026 (1997).
[31] S. C. Parida, S. K. Rakshit, and Z. Singh, J. Solid State Chem. **181**, 101 (2008).
[32] A. Zvezdin, Field induced phase transitions in ferrimagnets, in *Handbook of Magnetic Materials* (Elsevier, Amsterdam, 1995), Vol. 9, pp. 405–543.
[33] V. V. Yurlov, K. A. Zvezdin, G. A. Kichin, M. D. Davydova, A. E. Tseplina, N. T. Hai, J.-C. Wu, S.-Z. Ciou, Y.-R. Chiou, and L.-X. Ye, Appl. Phys. Lett. **116**, 222401 (2020).
[34] H. Leutwyler, Phys. Rev. D **49**, 3033 (1994).
[35] C. P. Hofmann, AIP Conf. Proc., **623**, 305 (2002).
[36] F. Hansteen, A. V. Kimel, A. Kirilyuk, and T. Rasing, Phys. Rev. Lett. **95**, 047402 (2005).
[37] F. Hansteen, A. V. Kimel, A. Kirilyuk, and T. Rasing, Phys. Rev. B **73**, 014421 (2006).